Chinese Journal of Structural Chemistry 45 (2026) 100766

Contents lists available at ScienceDirect

Chinese Journal of Structural Chemistry

journal homepage: www.journals.elsevier.com/chinese-journal-of-structural-chemistry

Article

An Al-based metal-organic framework with multiple gates for highly efficient separation of benzene/cyclohexene/cyclohexane

Wen-Yu Su[1], Fang-Di Dong[1], Zi-Luo Fang, Zhi-Shuo Wang, Mu-Yang Zhou, Xi Feng, Xiao-Tong Lu, Rong-Hua Wang, Xing-Yu Li, Dong-Dong Zhou*

MOE Key Laboratory of Bioinorganic and Synthetic Chemistry, GBRCE for Functional Molecular Engineering, School of Chemistry, IGCME, Sun Yat-Sen University, Guangzhou, 510275, China

ARTICLE INFO

Keywords:
Al-based metal-organic framework
Single crystals
Benzene/cyclohexene/cyclohexane mixture
Gating flexibility
Molecular sieving

ABSTRACT

Separation of ternary cyclic C_6 hydrocarbons, *i.e.*, the mixture of benzene (Bz), cyclohexene (Cye), and cyclohexane (Cya), is one of the critical chemical processes but challenging in the petrochemical industry. Here, we design and synthesize a stable Al-based metal-organic framework with high-quality single crystals, which exhibits excellent thermal stability (up to 300 °C), acid-base stability (within a pH range of 2–12) and boiling-water stability. Interestingly, by virtue of multiple gates controlled by organic fragments and/or inorganic clusters in the quasi-three-dimensional pores, the framework exhibits not only ultrahigh Bz/Cya (180) and Bz/Cye (66) selectivities, but also ultrahigh Bz selectivity (118) from the ternary Bz/Cye/Cya mixture. Notably, all the above selectivities rank in the top three in all porous materials, and the Bz/Cye selectivity is the highest to date. Single-crystal X-ray diffraction analyses and computational simulations revealed that the multiple types of gating play the crucial role in the adsorption and separation of Bz/Cye/Cya mixture.

1. Introduction

Hydrogenation of benzene (Bz) is one of the critical chemical processes, in which cyclohexene (Cye) as the partial hydrogenation product can be cleanly and efficiently converted into cyclohexanol via hydration reaction, serving as the vital raw material for the production of nylon-6 and nylon-66 [1,2]. Nevertheless, the generation of cyclohexane (Cya) is an inevitable byproduct in the synthesis of Cye [3–5]. Therefore, separation of the ternary cyclic C_6 mixture (Bz, Cye, and Cya) is required to obtain high-purity chemicals. However, they exhibit similar boiling points (Bz: 353.2 K; Cye: 356.0 K; Cya: 353.9 K) and form azeotropes, making the separation via conventional distillation inefficient [6,7]. While current extraction distillation employed in industrial settings involves complex operations, high energy consumption, and elevated costs [8]. Alternatively, adsorptive separation using porous materials offers a low-energy and cost-effective solution [9–13].

Porous coordination polymers (PCPs) or metal-organic frameworks (MOFs) exhibit significant potential for the separation of Bz and its analogues due to their high specific surface areas and tunable structures [14–18]. To our knowledge, most reported studies focus on binary Bz/Cya selectivity, whereas ternary Bz/Cya/Cye separation (more critical for industrial applications) remains underexplored [19–22]. Fortunately, by leveraging the flexibility of MOFs, particularly the gating flexibility, highly efficient separation of the ternary mixture could be achieved [23–25]. For example, $[Zn_2F_2(ebdim)]$ (MAF-55, H_2ebdim = 2,6-diethyl-benzo[1,2-*d*:4,5-*d*']diimidazole) with rotatable ethyl groups as the gate has achieved the benchmarked Bz/Cye/Cya selectivity (129), and $[Zn(btz)_2]$ (MAF-7Br, Hbtz = 3-bromo-1,2,4-triazole) with detachable and swingable C–Br···N halogen bonds as the gate has achieved the second highest selectivity (113). However, they have only one type of gate in the structure, and all the components of gates are constructed from organic fragments, which is also common in the gated-type MOFs.

As far as we know, Al(III) ions can form various building units (such as chains and rings) with carboxylate groups, which can be further connected by dicarboxylicates, tricarboxylicates, tetracarboxylicates, etc., to form stable Al-based MOF structures. Among them, there are specific pore apertures in the middle of these Al-ring clusters, such as

This article is part of a special issue entitled: Structural Chemistry published in Chinese Journal of Structural Chemistry.

* Corresponding author.
E-mail address: zhoudd3@mail.sysu.edu.cn (D.-D. Zhou).
[1] These authors contributed equally to this work.

https://doi.org/10.1016/j.cjsc.2025.100766
Received 14 August 2025; Received in revised form 3 October 2025; Accepted 6 October 2025
Available online 11 October 2025

eight-membered-ring (Al_8) and twelve-membered-ring (Al_{12}) clusters, which can also be used for adsorption and separation [26,27]. In other words, the center of multi-membered-ring Al_n cluster could also serve as a "gate" to separate mixtures. Moreover, due to their high stability [28, 29], low toxicity, low cost [30] and lightweight characteristics [31], Al-based MOFs exhibit extensive application prospects in adsorptive separation. However, examples with definitive structures are still limited, leading to the separation mechanism remaining unclear, because their large single crystals are difficult to obtain due to the strong Al–O bond and rapid growth rate of Al-MOF crystal nuclei [26].

Here, we design and synthesize a new Al-based MOF with high-quality single crystals under the modulation of chelidonic acid (H_2ca). Single-crystal X-ray diffraction (SCXRD) and theoretical calculations indicate that, by virtue of multiple types of gates (including organic fragments and inorganic clusters) in the quasi-three-dimensional (quasi-3D) pore channels, this MOF exhibits benchmarked selectivity for Bz from both binary and ternary mixtures.

2. Results and discussion

Solvothermal reaction of $Al_2(SO_4)_3{\cdot}18H_2O$, 4,4′-azanediyldibenzoic acid (H_2adb) and H_2ca in mixed solvents of *N*,*N*-dimethylformamide (DMF), water (H_2O) and formic acid (HCOOH) at 140 °C could afford colourless crystals of [Al(OH)(adb)]·Guest (**1**·**G**). It is worth noting that single crystals of **1**·**G** cannot be obtained in the absence of H_2ca, which indicated that H_2ca might act as a coordination regulator to slow down the nucleation rate of Al(III) ion [32,33], thereby facilitating the growth of single crystals. Moreover, microcrystalline samples of **1**·**G** could be synthesized in mixed solvents of DMF, H_2O and HCOOH at the same temperature for 24 h (Fig. S1).

SCXRD analysis of **1**·**G** showed that it crystallizes in the tetragonal crystal system with space group *I*422, comprising two Al(III) ions, one adb^{2-}, and one OH^- in the asymmetric unit (Fig. S2, and Table S1). Each Al(III) ion is coordinated by four oxygen atoms from four adb^{2-} ligands and two oxygen atoms from two bridging μ-OH^- groups, forming the AlO_6 polyhedron. Eight AlO_6 polyhedra are *cis*-connected via eight μ-OH^- groups to form an 8-membered-ring $[Al_8(OH)_8(RCOO)_{16}]$ cluster (Fig. 1(a)), which has already been observed in several Al-based MOFs [34]. Further, each $[Al_8(OH)_8(RCOO)_{16}]$ cluster connects with eight adjacent ones via sixteen adb^{2-} ligands, forming a 3D framework with a **bcu** topology (Fig. 1(a) and Fig. S3), which is isostructural with CAU-21 [35–37]. This connectivity generates two types of pores with void volume of 30.9% (Fig. 1(b)), one of which is 1D channels along the *c*-axis with two kinds of cavities (quadrangular-prism-shaped cavity I: 5.6 × 5.6 × 9.6 Å^3; ellipsoid-shaped cavity II: 6.6 × 8.7 × 8.7 Å^3, Fig. 1 (b)). Notably, there are two kinds of apertures in the 1D pore channel: aperture I–I is between two cavity I, which is the center of the $[Al_8(OH)_8(RCOO)_{16}]$ cluster (3.6 × 3.6 Å^2); aperture I–II is between cavity I and II formed by four phenyl rings (3.6 × 3.6 Å^2). Besides, the other cavities are regarded as quasi-discrete ones (cavity III: 3.9 × 8.5 × 8.6 Å^3) accompanied with four cavity I, with a very narrow aperture I–III (0.6 × 5.3 Å^2, Fig. 1(b) and Fig. S4).

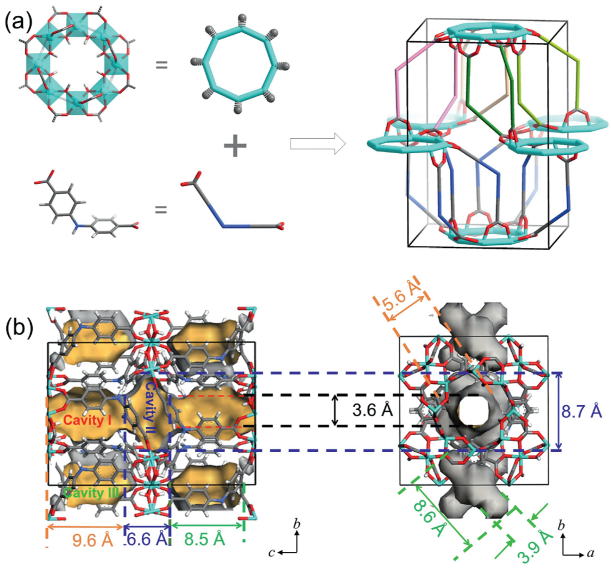

Fig. 1. Single-crystal structure of **1**. (a) 8-membered-ring $[Al_8(OH)_8(RCOO)_{16}]$ clusters and bent adb^{2-} ligands construct into the **bcu** framework of **1** (adb^{2-} ligands connecting the same two eight-membered rings are colored with the same color in the upper layer). (b) The pore structures viewed perpendicularly to (left) and along (right) the 1D channels.

Powder X-ray diffraction (PXRD) showed that **1**·**G** could be stable in aqueous solution with pH 2–12 and various common solvents, such as methanol (MeOH), ethanol, acetone, DMF, Bz, Cye, Cya and hexane, even in boiling water (Fig. S5). Thermogravimetric (TG) curves indicated that the guest in **1**·**G** could be exchanged by MeOH and the framework could be stable up to 300 °C (Fig. S6). Additionally, variable-temperature PXRD showed that the PXRD pattern of **1**·**G** after guest removal, that is guest-free **1**, almost unchanged before 300 °C (Fig. S7), suggesting that its framework appeared rigid. Additionally, the framework after Bz adsorption (denoted as Bz@**1**) was also proven to be isostructural with the as-synthesized structure, with no significant changes observed in the unit-cell parameters (Fig. S8, and Table S1). Interestingly, Bz molecules are present in all three cavities.

N_2 sorption isotherms of **1** at 77 K show that the uptake is 0.53 mmol g^{-1} at $P/P_0 = 0.9$, and negligible adsorption toward N_2 should be ascribed to the very small pore aperture [38,39]. CO_2 sorption isotherms of **1** at 195 K show the type-I adsorption behavior, indicating its typical microporous features. At $P/P_0 = 0.9$, the saturated uptake reached 5.8 mmol g^{-1} (Fig. S9), giving a pore volume of 0.230 cm^3 g^{-1}, which is close to the value calculated from the SCXRD structure (0.232 cm^3 g^{-1}). The Brunauer-Emmett-Teller (BET) and Langmuir surface area derived from the CO_2 isotherms are 331 and 439 m^2 g^{-1} (Fig. S10 and S11), respectively.

Single-component Bz, Cye, and Cya vapor sorption isotherms were performed at 298 K (Fig. 2(a)). The results showed that Bz exhibited obvious adsorption at low pressure (1.05 mmol g^{-1} at $P/P_0 = 0.05$), and the uptake increased slowly with increasing pressure, until it reached 2.09 mmol g^{-1} at $P/P_0 = 0.95$, which was close to the theoretical value (2.09 mmol g^{-1} or one molecule per cavity) obtained from grand canonical Monte Carlo (GCMC) simulations. For comparison, the uptake of Cye/Cya was 0.22/0.05 mmol g^{-1} at $P/P_0 = 0.05$ and 0.54/0.34 mmol g^{-1} at $P/P_0 = 0.95$, which was significantly less than that of Bz. In other words, the uptake ratios of Bz/Cye/Cya were 21:4.4:1 at 0.05 bar and 6.1:1.6:1 near 1 bar, indicating that the order of host-guest interactions follows Bz > Cye > Cya. Furthermore, differential scanning calorimetry (DSC) measurements revealed adsorption enthalpies (ΔH) of −72.3, −64.5, and −62.4 kJ mol^{-1} for Bz, Cye, and Cya (Fig. S12), respectively.

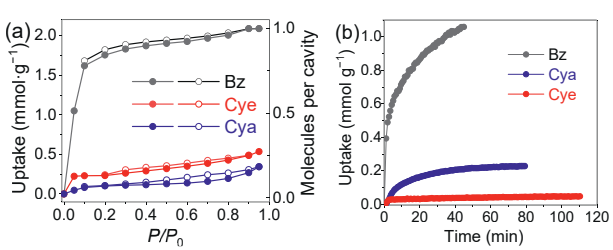

Fig. 2. Single-component sorption behaviors of Bz/Cye/Cya for **1** at 298 K. (a) Vapor adsorption (solid) and desorption (open) isotherms. (b) Adsorption kinetics at 0.05 bar.

To further investigate the adsorption behavior of the framework towards Bz, Cye and Cya, their kinetic data under 0.05 bar were analyzed. The results showed that Bz required ~45 min to reach adsorption equilibrium, with a diffusion coefficient constant of 0.176 h^{-1} (Fig. 2(b) and Fig. S13). However, Cye and Cya took ~80 and ~110 min to achieve equilibrium, yielding diffusion coefficients of 0.132 and 0.052 h^{-1}, respectively. This trend may arise from the narrow pore size of the framework and differences in guest molecule size/polarity. The calculated diffusion coefficient selectivity for Bz/Cye/Cya was determined to be 3.4/1.5/1. Additionally, although single-crystal samples exhibit the same gas adsorption behavior, they showed slower adsorption kinetics for Bz/Cye/Cya than those of microcrystalline sample, which should be ascribed to their larger particle sizes (Fig. S14–16) [40].

To verify the mixture separation performance, **1** was immersed in equimolar liquid mixtures of Bz/Cya, Bz/Cye, and Bz/Cye/Cya at 298 K. The acid digestion solutions of these samples were analyzed via gas chromatography (GC) and TG. The results showed selectivities of Bz/Cya, Bz/Cye, and Bz/Cye/Cya mixtures are 180(5), 65.7(2) and 118(4), respectively (Fig. 3(a), and Fig. S17 and S18), confirming the selective extraction of Bz from binary or ternary mixtures. As far as we know, the Bz selectivity in the binary/ternary mixtures belongs to the top three levels in all porous materials, and the Bz/Cye selectivity is the highest record (Fig. 3(b and c), and Table S2) [23,24,41]. Furthermore, the purity of desorbed Bz reached 98.3% from the ternary mixtures, demonstrating superior performance compared to many other porous materials. Moreover, the isostructural material CAU-21 with the same inorganic cluster gate and very similar organic fragments gate showed similar separation performance: Bz/Cye/Cya selectivity of 109, corresponding to the purity of 98.2% for Bz (Fig. S19 and S20). The cycling stability showed that the uptakes, Bz selectivity and PXRD pattern unchanged after 10-consecutive adsorption-desorption cycles, indicating the high stability and recyclability of **1** (Fig. 3(d) and Fig. S21).

To further investigate the host-guest interactions, multiple computational simulations were carried out. First, GCMC simulations demonstrated that each cavity in **1** can accommodate one Bz, Cye and Cya molecule, respectively, corresponding to a theoretical saturated uptake of 2.09 mmol g^{-1}. Moreover, the adsorption position of Bz is consistent with the SCXRD structure (Fig. S22). Furthermore, periodic density functional theory (PDFT) calculations showed the preferential adsorption sites for both of the three guests locate in cavity I, with the ΔH of

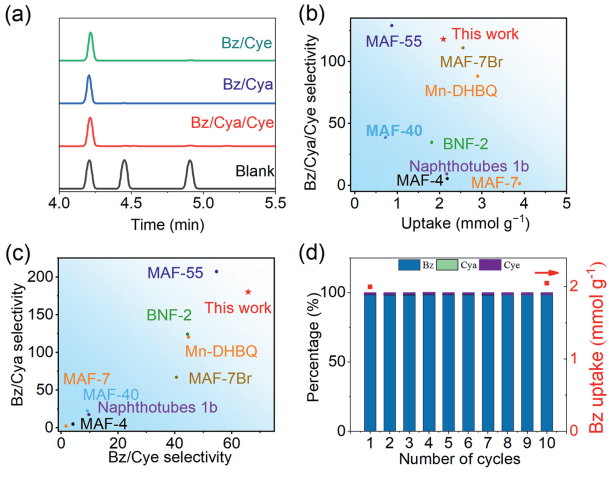

Fig. 3. Mixture adsorption and separation results. (a) Typical GC traces of the digestion solutions of **1** after soaking in equimolar mixtures of Bz/Cye (up), Bz/Cya (middle), and Bz/Cya/Cye (down). (b) Comparison of Bz/Cya/Cye selectivities and uptakes for typical MOFs. (c) Comparison of Bz/Cya and Bz/Cye selectivities of typical MOFs. (d) Adsorption-desorption cycles in equimolar Bz/Cye/Cya mixtures.

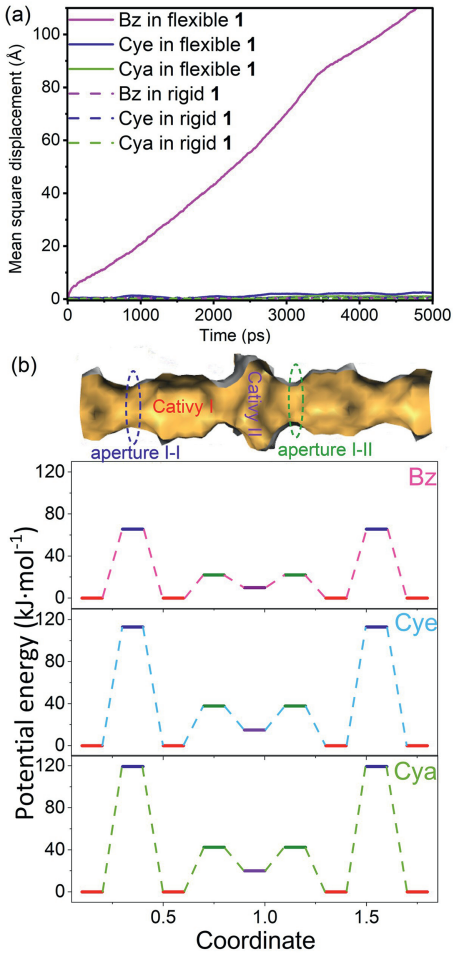

Fig. 4. Simulated adsorption kinetic results. (a) MD-derived self-diffusion rates of Bz/Cye/Cya. (b) The energy barriers for Bz (up), Cye (middle) and Cya (down) through the 1D pore channel (up).

−79.6/−67.9/−63.1 kJ mol^{-1} for Bz/Cye/Cya, respectively (Fig. S23). Obviously, Bz shows significantly stronger interaction than that of Cye/Cya, which is consistent with the DSC. Specifically, two C–H···π interactions (H···π 2.805/2.840 Å) and four π···π interactions (3.390–3.440 Å) exist in Bz@**1**, while only four C–H···π interactions exist (H···π 2.429–2.789 Å) in Cye@**1** and four C–H···π interactions (H···π 2.606–2.658 Å) in Cya@**1** (Fig. S24 and Table S3).

Molecular dynamics (MD) simulations were performed to investigate the diffusion dynamics of individual Bz, Cye, and Cya guest. Expectably, if the host was set rigid, the diffusion of Bz/Cye/Cya was forbidden (< 1.1×10^{-13} m^2 s^{-1}) in **1** (Fig. 4(a), and Fig. S25 and Table S4). When the host was set flexible, Bz, Cya and Cye could diffuse in the 1D pore channel (including aperture I–II and I–I) of **1**, in which Bz diffuses significantly faster, 1.7×10^{-9}, 4.4×10^{-12} and 3.4×10^{-12} m^2 s^{-1} for Bz, Cya and Cye (Fig. S26), respectively. Furthermore, the result showed that the energy barriers of Bz/Cye/Cya through aperture I–I and I–II are 65.5/113.0/119.4 kJ mol^{-1} and 22.0/37.8/42.5 kJ mol^{-1}, respectively (Fig. 4(b)), indicating that guest passing through the aperture I–I is likely to be the rate-determining step. This is because aperture I–I is an 8-membered-ring $[Al_8(OH)_8(RCOO)_{16}]$ cluster, which is relatively more rigid, making it more difficult for guests to diffuse.

3. Conclusion

In summary, we report a new single-crystal structure of Al-based MOF with quasi-3D pore channels. By virtue of these multiple types of

gates in the structure, the MOF exhibits ultrahigh selectivity for Bz from both binary and ternary Bz/Cye/Cya mixtures. SCXRD and theoretical simulations demonstrated the inorganic Al_8 controlled gate played the crucial role in the Bz/Cye/Cya separation. This work not only provides a new approach for efficiently separating ternary cyclic C_6 hydrocarbons, but also offers new insights into the design of porous structures with gating behaviors for adsorptive separation.

4. Experimental

4.1. Materials and methods

All chemicals were purchased from a commercial source and used without further purification. Elemental analyses (EA) were performed by a Vario EL elemental analyzer (C, H and N). PXRD patterns were carried out with a Rigaku SmartLab diffractometer. TG analyses were carried out using a TA TGA 55 instrument in nitrogen flow with a heating rate of 5 °C min^{-1}. The sorption isotherms were measured with an automatic volumetric adsorption apparatus (ASAP 2020 M). Bz/Cye/Cya adsorption and desorption isotherms were collected by a BSD-VVS&DVS gravimetric adsorption analyzer (Beishide Instrument Technology (Beijing) Co., China). The equilibrium condition for vapor isotherms is weight change no more than 0.1 mg per 30 min [42].

4.2. Synthesis of 1·G

The mixture of $Al_2(SO_4)_3{\cdot}18H_2O$ (117.3 mg, 0.176 mmol), H_2adb (75.8 mg, 0.176 mmol), H_2ca (40 mg, 0.217 mmol), DMF (2 mL), H_2O (2 mL) and HCOOH (150 μL) was sealed in a Teflon-lined reactor and heated at 140 °C for 12 h, then cooled to room temperature at a rate of 10 °C h^{-1}. Colourless crystals of **1·G** were collected by filtration, washed three times with MeOH (10 mL), and dried under vacuum. Microcrystals of **1·G** could be synthesized by mixing $AlCl_3{\cdot}6H_2O$ (0.118 g, 0.7 mmol), H_2adb (0.18 g, 0.7 mmol) and HCOOH (300 μL) in a solvent mixture of DMF (3 mL) and H_2O (0.75 mL) under stirring conditions and heating at 140 °C for 24 h, then white microcrystalline sample of **1·G** was obtained after filtration, washed with DMF and H_2O, and dried under air (100 mg, yield: ~48%). For subsequent characterization, the sample was exchanged by MeOH for six times, and heated at 100 °C under vacuum. To facilitate storage, the sample was stored in air, which might adsorb a small amount of H_2O. Unless otherwise specified, microcrystalline samples were used for all measurements. EA calculated (%) for [Al(OH)(adb)]·2.2H_2O ($C_{14}H_{13.4}NAlO_{7.2}$): C, 49.77; H, 3.99; N, 4.15. Found (%): C, 49.85; H, 3.88; N, 4.06.

4.3. Crystal structures determination

SCXRD data of **1·G** and Bz@**1** were collected on a Rigaku XtaLAB Synergy Custom single-crystal diffractometer by using graphite monochromated Cu-Kα radiation, with absorption corrections applied by using the multi-scan program CrysAlisPro. The structure was solved by direct methods using SHELXT and refined with a full-matrix least-squares on F^2 using SHELXL. Anisotropic thermal parameters were applied to all non-hydrogen atoms, and all the hydrogen atoms were generated geometrically. The Solvent Mask treatment was applied for **1·G** because the guest molecules are extremely disordered and cannot be modelled. CCDC 2479746 and 2479747 contain the supplementary crystallographic data for this paper. These data are provided free of charge by the joint Cambridge Crystallographic Data Centre via www.ccdc.cam.ac.uk/data_request/cif. Single-crystal data and details of refinements are summarized in Table S1.

4.4. Mixture adsorption and separation experiments

The activated **1** sample (~200 mg) was introduced into binary or ternary liquid mixtures and sealed in an oven at 298 K. After 1 h, the sample was filtered and purged by nitrogen (20 mL min^{-1}, RT) for 30 min to eliminate residual solvents. Then ~10 mg sample was taken out and digested by using nitric acid or hydrochloric acid, followed by three sequential extractions using *n*-hexane (0.5 mL for each). The combined organic phases (1.5 mL total) were analyzed via GC-MS. The remaining sample (non-digested) was subjected to thermal regeneration under vacuum at 120 °C for 3 h for the next adsorption. The adsorption and desorption procedures in mixed systems were repeated for ten consecutive adsorption-desorption cycle experiments.

4.5. Calculation of diffusional time constant

The diffusional time constant D' was calculated from the following equation [43]:

$$\frac{q_t}{q_\infty} = \frac{6}{\sqrt{\pi}} \times \sqrt{\frac{D}{r^2} \times t}$$

$$D' = \frac{D}{r^2} = \frac{\left(\frac{q_t}{q_\infty}\right)^2 \times \frac{\pi}{36}}{t}$$

where q_t is the gas uptake at time t, q_∞ is the uptake at equilibrium, D is the diffusivity and r is the radius of the equivalent spherical particle.

4.6. Gas chromatography-mass spectrometry analyses

The Bz/Cya, Bz/Cye, and Bz/Cye/Cya ratios in the digestion solutions were analyzed on an Agilent 7890A GC system equipped with an Agilent 5975C insert mass spectrometer (MS) and an Agilent CP Sil 5 CB chromatographic column. For each GC injection, 1 μL aliquot of analytes was injected in manual. The data acquisition and processing were controlled by the Agilent 5975C Data Analysis software.

The purity of component i was calculated by the equation:

$$p_i = \frac{A_i}{A_1 + \cdots + A_i} \times 100\%$$

where A_i is the peak areas of component i.

The selectivity (S) was calculated by the equation [42]:

$$S = \frac{A_2/(A_1 + \cdots + A_i\text{–}A_2)}{A_i'/(A_1' + \cdots + A_i'\text{–}A_2')}$$

where A_i and A_i' are the peak areas of component i in the extract and blank equimolar samples, respectively.

4.7. Computational simulations

All simulations/calculations were performed using the Materials Studio 5.5 package. The guest adsorption was generated from GCMC simulations at 298 K in the Sorption module. For GCMC simulation, the Metropolis method and dreiding field were used [44]. All the charges of atoms were adopted by Mulliken charges, which were calculated from PDFT, and the cutoff radius was chosen as 18.5 Å for the Lennard-Jones (LJ) potential. The electrostatic interactions and van der Waals interactions were handled using the Ewald and Atom based summation methods, respectively, and all the equilibration steps and production steps were set as 1×10^7.

PDFT calculations were performed by the Dmol^3 module. All geometry optimizations used the generalized gradient approximation (GGA) with the Perdew-Burke-Ernzerhof (PBE) functional and the double numerical plus d-functions (DNP) basis set [45]. The Grimme method was used for DFT-D correction, and effective core potentials (ECP) for core treatment were applied. The energy, gradient, and displacement convergence criteria were set as 1×10^{-5} Ha, 2×10^{-3} Å, and 5×10^{-3} Å, respectively. The host framework and the guest

molecule were both regarded as flexible, and the ΔH was calculated by $\Delta H = E_{host\ +\ guest} - E_{host} - E_{guest}$ (the E_{host}, E_{guest} and $E_{host\ +\ guest}$ are the energies of the host, guest and the energies of the final host-guest system, respectively) [46].

MD simulations were performed in the Forcite module. The initial configurations for the MD simulations were produced by the GCMC loading results followed by global geometry optimizations through the dreiding field. All of the MD processes adopted the canonical ensemble with constant volume/temperature (NVT) using Nose thermostat and random initial velocities [47]. The time step was 1.0 fs and total simulation time was 5 ns. The electrostatic interactions and van der Waals interactions were evaluated by the Ewald summation method, with a Buffer width of 0.5 Å. The first 2 ns was used as equilibrium and the following 2 ns was adopted for statistical analysis such as for mean square displacements.

CRediT authorship contribution statement

Wen-Yu Su: Writing – original draft, Investigation, Formal analysis, Data curation. **Fang-Di Dong:** Investigation, Formal analysis, Data curation. **Zi-Luo Fang:** Investigation. **Zhi-Shuo Wang:** Investigation. **Mu-Yang Zhou:** Investigation. **Xi Feng:** Investigation. **Xiao-Tong Lu:** Investigation. **Rong-Hua Wang:** Investigation. **Xing-Yu Li:** Methodology. **Dong-Dong Zhou:** Writing – review & editing, Supervision, Funding acquisition, Conceptualization.

Declaration of competing interest

There are no conflicts to declare.

Acknowledgements

This work was supported by the National Natural Science Foundation of China (Nos. 22475240, 22090061, and 22488101). The authors thank Prof. Jie-Peng Zhang and Prof. Xiao-Ming Chen for helpful discussion.

Appendix A. Supplementary data

Supplementary data to this article can be found online at https://doi.org/10.1016/j.cjsc.2025.100766.

References

[1] F. Chavarria, D.R. Paul, Comparison of nanocomposites based on nylon 6 and nylon 66, Polymer 45 (2004) 8501–8515.
[2] C. Chen, H.-Y. Guan, H.-B. Li, Y.-Z. Zhou, Y.-G. Huang, W. Wei, M.-C. Hong, M.-Y. Wu, A noncovalent π-stacked porous organic molecular framework for selective separation of aromatics and cyclic aliphatics, Angew. Chem. Int. Ed. 61 (2022) e202201646.
[3] J.P.G. Villaluenga, A. Tabe-Mohammadi, A review on the separation of benzene/cyclohexane mixtures by pervaporation processes, J. Membr. Sci. 169 (2000) 159–174.
[4] L. Foppa, J. Dupont, Benzene partial hydrogenation: advances and perspectives, Chem. Soc. Rev. 44 (2015) 1886–1897.
[5] P. Zhang, T.-B. Wu, T. Jiang, W.-T. Wang, H.-Z. Liu, H.-L. Fan, Z.-F. Zhang, B.-X. Han, Ru–Zn supported on hydroxyapatite as an effective catalyst for partial hydrogenation of benzene, Green Chem. 15 (2013) 152–159.
[6] D.S. Sholl, R.P. Lively, Seven chemical separations to change the world, Nature 532 (2016) 435–437.
[7] P. Navarro, A. Ovejero-Pérez, M. Ayuso, N. Delgado-Mellado, M. Larriba, J. García, F. Rodríguez, Cyclohexane/cyclohexene separation by extractive distillation with cyano-based ionic liquids, J. Mol. Liq. 289 (2019) 111120.
[8] W. Zhang, W. Zhao, S. Ren, Y. Hou, W. Wu, Highly efficient separation of benzene + cyclohexane mixtures by extraction combined extractive distillation using imidazolium-based dicationic ionic liquids, Green Chem. Eng. 4 (2023) 312–323.
[9] D.J. O'Hearn, A. Bajpai, M.J. Zaworotko, The "Chemistree" of porous coordination networks: taxonomic classification of porous solids to guide crystal engineering studies, Small 17 (2021) 2006351.
[10] S. Mukherjee, D. Sensharma, O.T. Qazvini, S. Dutta, L.K. Macreadie, S.K. Ghosh, R. Babarao, Advances in adsorptive separation of benzene and cyclohexane by metal-organic framework adsorbents, Coord. Chem. Rev. 437 (2021) 213852.
[11] H.-M. Yang, L.-H. Xue, X.-G. Yang, H. Xu, J.-K. Gao, Advances in metal-organic frameworks for efficient separation and purification of natural gas, Chin. J. Struct. Chem. 42 (2023) 100034.
[12] M. Dincă, J.R. Long, Introduction: porous framework chemistry, Chem. Rev. 120 (2020) 8037–8038.
[13] N. Kumar, S. Mukherjee, A.A. Bezrukov, M. Vandichel, M. Shivanna, D. Sensharma, A. Bajpai, V. Gascón, K.-I. Otake, S. Kitagawa, M.J. Zaworotko, A square lattice topology coordination network that exhibits highly selective C_2H_2/CO_2 separation performance, SmartMat 1 (2020) e1008.
[14] J. Yan, H.-Y. Sun, Q.-L. Wang, L. Lu, B. Zhang, Z.-G. Wang, S.-W. Guo, F.-L. Han, Covalent triazine frameworks for the dynamic adsorption/separation of benzene/cyclohexane mixtures, New J. Chem. 46 (2022) 7580–7587.
[15] H. Ni, Y. Wang, K. Yao, L. Wang, J. Huang, Y. Xiao, H. Chen, B. Liu, C.Y. Yang, J. Zhao, Cyclical palmitoylation regulates TLR9 signalling and systemic autoimmunity in mice, Nat. Commun. 15 (2024) 1.
[16] L.-G. Hu, W.-H. Wu, M. Hu, L. Jiang, D.-H. Lin, J. Wu, K. Yang, Double-walled Al-based MOF with large microporous specific surface area for trace benzene adsorption, Nat. Commun. 15 (2024) 3204.
[17] Y. Han, W. Huang, M. He, B. An, Y. Chen, X. Han, L. An, M. Kippax-Jones, J. Li, Y. Yang, M.D. Frogley, C. Li, D. Crawshaw, P. Manuel, S. Rudić, Y. Cheng, I. Silverwood, L.L. Daemen, A.J. Ramirez-Cuesta, S.J. Day, S.P. Thompson, B. F. Spencer, M. Nikiel, D. Lee, M. Schröder, S. Yang, Trace benzene capture by decoration of structural defects in metal-organic framework materials, Nat. Mater. 23 (2024) 1531–1538.
[18] S. Horike, S. Kitagawa, The development of molecule-based porous material families and their future prospects, Nat. Mater. 21 (2022) 983–985.
[19] F. Xie, L. Yu, T. Jenkins, T. Thonhauser, H. Wang, J. Li, Flexible layered metal-organic framework for temperature-dependent discrimination of cyclic hydrocarbons, ACS Mater. Lett. 7 (2025) 780–786.
[20] Y. Han, Y. Chen, Y. Ma, J. Bailey, Z. Wang, D. Lee, A.M. Sheveleva, F. Tuna, E.J. L. McInnes, M.D. Frogley, S.J. Day, S.P. Thompson, B.F. Spencer, M. Nikiel, P. Manuel, D. Crawshaw, M. Schröder, S. Yang, Control of the pore chemistry in metal-organic frameworks for efficient adsorption of benzene and separation of benzene/cyclohexane, Chem 9 (2023) 739–754.
[21] R.-C. Zhao, L.-H. Xie, X.-M. Liu, Z. Liu, X.-Y. Li, J.-R. Li, Removal of trace benzene from cyclohexane using a MOF molecular sieve, J. Am. Chem. Soc. 147 (2025) 2467–2475.
[22] C.-H. Liu, L. Chen, H. Zhang, Y. Li, H. Lin, L. Li, J. Wu, C. Liu, Z.-M. Ye, S. Xiang, B. Chen, Z. Zhang, A B←N framework based on 1D dative B←N polymers for exclusive recognition and separation of benzene from its azeotrope, Chem 9 (2023) 3532–3543.
[23] D.-D. Zhou, X. Feng, D.-Y. Hu, X.-T. Lu, F.-D. Dong, Z.-L. Fang, R.-B. Lin, J.-P. Zhang, X.-M. Chen, Inversed benzene/cyclohexene/cyclohexane adsorption selectivities for one-step purification of cyclohexene and beyond, J. Am. Chem. Soc. 147 (2025) 17342–17349.
[24] Z.-J. Liang, F.-D. Dong, L. Ye, K. Zheng, D.-Y. Hu, X. Feng, W.-Y. Su, Z.-S. Wang, M.-Y. Zhou, Z.-L. Fang, D.-D. Zhou, J.-P. Zhang, X.-M. Chen, Introducing halogen-bonded gates into zeolitic frameworks for efficient benzene/cyclohexene/cyclohexane separation, Chem. Sci. 16 (2025) 3307–3312.
[25] X. Feng, D.-Y. Hu, Z.-J. Liang, M.-Y. Zhou, Z.-S. Wang, W.-Y. Su, R.-B. Lin, D.-D. Zhou, J.-P. Zhang, A metal azolate framework with small aperture for highly efficient ternary benzene/cyclohexene/cyclohexane separation, Chin. J. Struct. Chem. 44 (2025) 100540.
[26] W.-D. Fan, K.-Y. Wang, C. Welton, L. Feng, X.-K. Wang, X.-P. Liu, Y. Li, Z.-X. Kang, H.-C. Zhou, R.-M. Wang, D.-F. Sun, Aluminum metal-organic frameworks: from structures to applications, Coord. Chem. Rev. 489 (2023) 215175.
[27] E. Alvarez, N. Guillou, C. Martineau, B. Bueken, B. Van de Voorde, C. Le Guillouzer, P. Fabry, F. Nouar, F. Taulelle, D. de Vos, J.-S. Chang, K.H. Cho, N. Ramsahye, T. Devic, M. Daturi, G. Maurin, C. Serre, The structure of the aluminum fumarate metal-organic framework A520, Angew. Chem. Int. Ed. 54 (2015) 3664–3668.
[28] M. Gaab, N. Trukhan, S. Maurer, R. Gummaraju, U. Müller, The progression of Al-based metal-organic frameworks — from academic research to industrial production and applications, Microporous Mesoporous Mater. 157 (2012) 131–136.
[29] T. Loiseau, L. Lecroq, C. Volkringer, J. Marrot, G. Férey, M. Haouas, F. Taulelle, S. Bourrelly, P.L. Llewellyn, M. Latroche, MIL-96, a porous aluminum trimesate 3D structure constructed from a hexagonal network of 18-membered rings and μ_3-oxo-centered trinuclear units, J. Am. Chem. Soc. 128 (2006) 10223–10230.
[30] T.-R. Wu, N. Prasetya, K. Li, Recent advances in aluminium-based metal-organic frameworks (MOF) and its membrane applications, J. Membr. Sci. 615 (2020) 118493.
[31] X.-L. Si, C.-L. Jiao, F. Li, J. Zhang, S. Wang, S. Liu, Z.-B. Li, L.-X. Sun, F. Xu, Z. Gabelica, C. Schick, High and selective CO_2 uptake, H_2 storage and methanol sensing on the amine-decorated 12-connected MOF CAU-1, Energy Environ. Sci. 4 (2011) 4522–4527.
[32] S. Canossa, A. Gonzalez-Nelson, L. Shupletsov, M. del Carmen Martin, M.A. Van der Veen, Overcoming crystallinity limitations of aluminium metal-organic frameworks by oxalic acid modulated synthesis, Chem. Eur. J. 26 (2020) 3564–3570.
[33] L.-M. Cui, W.-H. Fang, J. Zhang, Polyoxometalates containing aluminum atoms, Chin. Chem. Lett. 36 (2025) 110386.
[34] N. Stock, High-throughput investigations employing solvothermal syntheses, Microporous Mesoporous Mater. 129 (2010) 287–295.
[35] M. Krüger, A.K. Inge, H. Reinsch, Y.-H. Li, M. Wahiduzzaman, C.-H. Lin, S.-L. Wang, G. Maurin, N. Stock, Polymorphous Al-MOFs based on V-shaped linker

molecules: synthesis, properties, and *in situ* investigation of their crystallization, Inorg. Chem. 56 (2017) 5851–5862.
[36] F. Gándara, H. Furukawa, S. Lee, O.M. Yaghi, High methane storage capacity in aluminum metal-organic frameworks, J. Am. Chem. Soc. 136 (2014) 5271–5274.
[37] C.-S. Liu, C.-X. Sun, J.-Y. Tian, Z.-W. Wang, H.-F. Ji, Y.-P. Song, S. Zhang, Z.-H. Zhang, L.-H. He, M. Du, Highly stable aluminum-based metal-organic frameworks as biosensing platforms for assessment of food safety, Biosens. Bioelectron. 91 (2017) 804–810.
[38] D.-F. Lv, Y. Wu, J.-Y. Chen, Y.-H. Tu, Y.-N. Yuan, H.-X. Wu, Y.-W. Chen, B.-Y. Liu, H.-X. Xi, Z. Li, Q.-B. Xia, Improving CH_4/N_2 selectivity within isomeric Al-based MOFs for the highly selective capture of coal-mine methane, AlChE J. 66 (2020) e16287.
[39] L. Yu, S. Ullah, J.-Z. Yao, D.-X. Lin, J.-J. Huang, S. Tu, H.-Y. Luo, Q.-B. Xia, T. Thonhauser, H. Wang, Full exclusion of branched hexanes from their linear isomer by a robust aluminum metal-organic framework with tailored pore structure, ACS Mater. Lett. 5 (2023) 1532–1536.
[40] L.-H. Yang, Y. Liu, F. Zheng, F.-X. Shen, B.-J. Liu, Rajamani Krishna, Z.-G. Zhang, Q.-W. Yang, Q.-L. Ren, Z.-B. Bao, Leveraging diffusion kinetics to reverse propane/propylene adsorption in zeolitic imidazolate framework-8, ACS Nano 18 (2024) 3614–3626.
[41] F. Xie, L.-H. Chen, E.M. C. Morales, S. Ullah, Y.-W. Fu, T. Thonhauser, K. Tan, Z.-B. Bao, J. Li, Complete separation of benzene-cyclohexene-cyclohexane mixtures via temperature-dependent molecular sieving by a flexible chain-like coordination polymer, Nat. Commun. 15 (2024) 2240.
[42] M.-Y. Zhou, X.-W. Zhang, H. Yi, Z.-S. Wang, D.-D. Zhou, R.-B. Lin, J.-P. Zhang, X.-M. Chen, Molecular-sieving separation of methanol/benzene azeotrope by a flexible metal-organic framework, J. Am. Chem. Soc. 146 (2024) 12969–12975.
[43] Z.-M. Ye, X.-F. Zhang, D.-X. Liu, Y.-T. Xu, C. Wang, K. Zheng, D.-D. Zhou, C.-T. He, J.-P. Zhang, A gating ultramicroporous metal-organic framework showing high adsorption selectivity, capacity and rate for xylene separation, Sci. China Chem. 65 (2022) 1552–1558.
[44] K. Sasaki, T. Yamashita, Modification and validation of the DREIDING force field for molecular liquid simulations (DREIDING-UT), J. Chem. Inf. Model. 61 (2021) 1172–1179.
[45] D.-D. Zhou, P. Chen, C. Wang, S.-S. Wang, Y. Du, H. Yan, Z.-M. Ye, C.-T. He, R.-K. Huang, Z.-W. Mo, N.-Y. Huang, J.-P. Zhang, Intermediate-sized molecular sieving of styrene from larger and smaller analogues, Nat. Mater. 18 (2019) 994–998.
[46] X.-W. Zhang, D.-D. Zhou, J.-P. Zhang, Tuning the gating energy barrier of metal-organic framework for molecular sieving, Chem 7 (2021) 1006–1019.
[47] Z.-F. Jiang, W.-J. Xue, H.-L. Huang, H.-J. Zhu, Y.-X. Sun, C.-L. Zhong, Mechanochemistry-assisted linker exchange of metal-organic framework for efficient kinetic separation of propene and propane, Chem. Eng. J. 454 (2023) 140093.